Chemical Science

ROYAL SOCIETY OF CHEMISTRY

EDGE ARTICLE

View Article Online
View Journal | View Issue

Cite this: *Chem. Sci.*, 2025, **16**, 14681

All publication charges for this article have been paid for by the Royal Society of Chemistry

Received 2nd April 2025
Accepted 9th July 2025

DOI: 10.1039/d5sc02492g

rsc.li/chemical-science

2D-to-3D transformations of a covalent organic framework *via* post-synthetic crosslinking†

Garrison A. Bauer and Mercedes K. Taylor *

Two-dimensional (2D) covalent organic frameworks (COFs) are easier to synthesize and functionalize than their three-dimensional (3D) counterparts, but the 2D frameworks lack stability due to weak non-covalent interactions that maintain the layered structure. Herein, we provide a post-synthetic strategy to covalently crosslink the independent sheets of 2D COFs while preserving the crystallinity and porosity of the materials. The crosslinked frameworks show greatly enhanced mechanical stability compared to the parent 2D frameworks, retaining more than 90% of the original Brunauer–Emmett–Teller (BET) surface area when subjected to extensive sonication or grinding. Further, crosslinking enables the reduction of the imine linkages with sodium borohydride while preserving crystallinity and porosity, which has yet to be shown for 2D COFs. Finally, the imine linkages on a crosslinked framework were first reduced and then reacted with an acyl chloride, establishing a general approach to framework functionalization. This post-synthetic crosslinking approach stabilizes 2D frameworks and opens access to amine linkages in these materials, thus increasing hydrolytic stability and potential functionalization as selective adsorbents.

Introduction

Covalent organic frameworks (COFs) are a class of porous, crystalline materials that are highly tunable but inherently fragile due to the reversible linkages between monomers.[1,2] Depending on the geometry of the monomers, framework synthesis results in two-dimensional (2D) sheets or three-dimensional (3D) networks.[3,4] Perhaps due to the ease of monomer synthesis, 2D COFs have been studied more extensively and have yielded a broader library of structures than have 3D COFs.[5] Further, the 2D frameworks can tolerate a relatively wide range of functional groups on the monomers, while such functionality often prevents the formation of a corresponding 3D framework.[6–8]

Despite these advantages, the industrial application of 2D COFs is hindered by their chemical and mechanical instability. Unlike 3D frameworks, the stacked sheets of the 2D materials are held together by weak, non-covalent interactions, mainly π–π stacking.[5,8] Consequently, these materials exhibit interlayer slipping from exposure to solvents or various guests, decreasing porosity and thermal stability.[9–11] Under harsher conditions such as grinding or sonication, complete disruption of the interlayer interactions can occur, causing exfoliation of the layers.[12–14] These structural distortions cause a loss of crystallinity and porosity, hindering the performance of the material.[15]

Further, the instability of 2D COFs limits the linkage transformations that are possible for these materials. As we and others have shown, the reduction of imine linkages in 3D frameworks with sodium borohydride ($NaBH_4$) improves hydrolytic stability and opens the door to linkage functionalization.[6,16,17] However, applying these reduction conditions to analogous 2D frameworks results in substantial loss of crystallinity and complete loss of porosity.[18–20]

Among the various efforts to increase the stability of 2D frameworks,[21–26] a unique and promising strategy is to covalently link neighboring layers. In 2021, Perepichka and coworkers crosslinked a vinylene-linked 2D framework *via* a [2 + 2] cycloaddition, forming interlayer C–C bonds, but the cycloaddition was shown to be reversible upon heating.[27] In 2023, Zhang and coworkers synthesized a crosslinked 2D framework using pre-linked monomers. The resulting materials showed increased mechanical stability, but the fact that the monomers were tethered to each other as dimers during framework synthesis prevented the formation of highly crystalline materials.[15]

Instead, we hypothesized that a 2D-to-3D transformation based on irreversible post-synthetic crosslinking would allow us to maximize stability without sacrificing crystallinity. We note that because COFs are insoluble solids, post-synthetic crosslinking occurs as a solid-state transformation. By reacting a difunctional guest molecule with pendant functional groups on the pore walls, we aimed to covalently crosslink independent layers of a 2D framework. We hypothesized that by using relatively short alkyl spacers between the reactive end groups of the crosslinker, the crosslinking molecules would link adjacent

Department of Chemistry and Biochemistry, University of Maryland, College Park, MD 20742, USA. E-mail: mkt@umd.edu

† Electronic supplementary information (ESI) available. See DOI: https://doi.org/10.1039/d5sc02492g

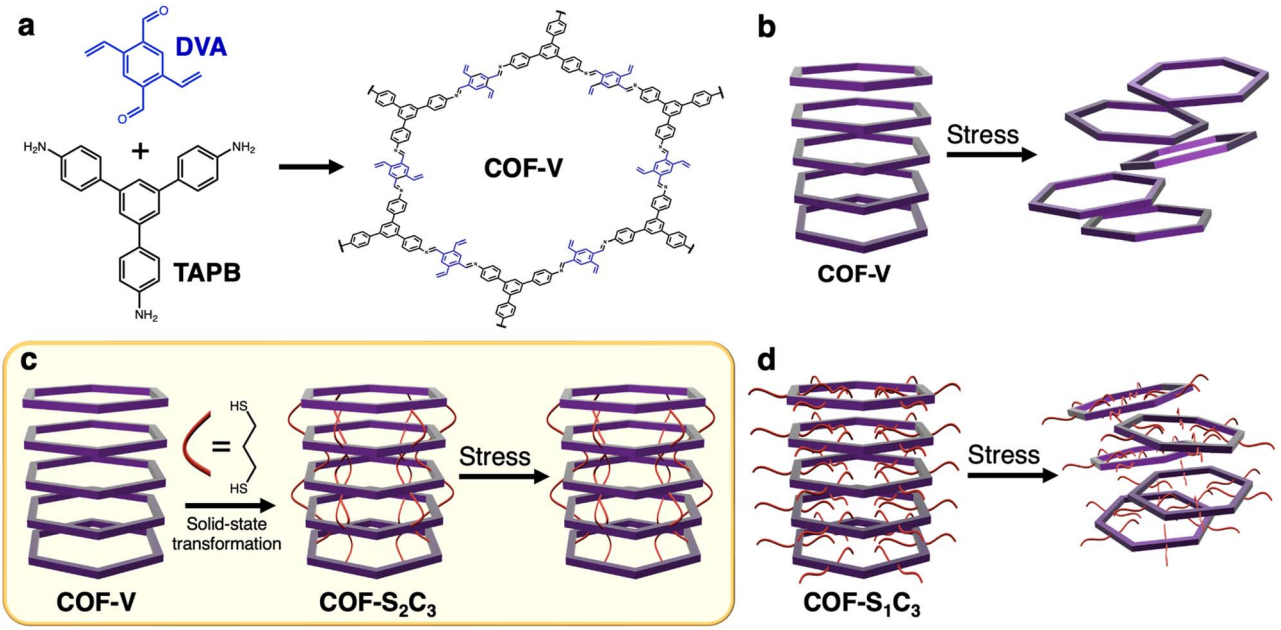

Scheme 1 Synthesis and stability testing of COF-V (a and b), COF-S_2C_3 (c), and COF-S_1C_3 (d).

layers without bridging pores or significantly reducing surface area. Ultimately, we envisioned that such short, strong crosslinks would prevent layer slippage and exfoliation in response to chemical or mechanical stress.

Herein, we report the first irreversible crosslinking of an imine-linked framework *via* post-synthetic modification (Scheme 1). We synthesized a vinyl-appended framework termed COF-V and reacted dithiol crosslinkers with vinyl groups on the framework walls through the thiol–ene click reaction.[28] The frameworks were then subjected to mechanical stability testing by sonication and grinding and to chemical stability testing by reaction with $NaBH_4$, none of which resulted in framework degradation. This is the first report of the reduction of a 2D framework with $NaBH_4$ while retaining significant crystallinity and porosity. The reduced linkages were then used as reactive sites for further functionalization with acetyl chloride. The simple crosslinking method reported here produces highly stable materials, enabling 2D frameworks to be used in harsh industrial conditions and readily tailored for desired separations.

Results and discussion

The known framework COF-V was synthesized through the condensation of 2,5-divinylterephthalaldehyde (DVA)[29–31] and 1,3,5-tris-(4-aminophenyl)benzene (TAPB),[32] which were combined with 12 M acetic acid in acetonitrile for three days at room temperature (Scheme 1a).[33] The purity of the synthesized monomers and molecular analogues was confirmed by ^{1}H NMR (Fig. S1–S5†). Fourier-transform infrared (FTIR) spectroscopy was used to confirm the conversion of aldehydes and amines to imine functional groups (Fig. S6†). The appearance of the imine signal at 1620 cm^{-1}, along with the disappearance of the aldehyde signal at 1685 cm^{-1} and amine signals at 3430 cm^{-1} and 3350 cm^{-1}, show the formation of an imine-linked material. Powder X-ray diffraction (PXRD) data (Fig. S7†) and N_2 adsorption data (Fig. S8†) confirmed the formation of the desired framework.

Although the as-synthesized COF-V is crystalline and porous, the framework is readily damaged by harsh mechanical or chemical treatment, as discussed further below (Scheme 1b). To address this instability, the vinyl groups of COF-V were reacted with a series of dithiols increasing in alkyl chain length: 1,2-ethanedithiol (abbreviated herein as S_2C_2), 1,3-propanedithiol (abbreviated herein as S_2C_3), or 1,4-butanedithiol (abbreviated herein as S_2C_4). The resulting crosslinked materials are termed COF-S_2C_2, COF-S_2C_3, and COF-S_2C_4 (Scheme 1c). As a control, a non-crosslinked material was synthesized by reacting COF-V with 1-propanethiol (abbreviated herein as S_1C_3) to yield COF-S_1C_3 (Scheme 1d).

The selection of dithiol crosslinkers was based on a structural model of COF-V that we constructed with the program Materials Studio, which showed the distance between interlayer vinyl groups to be 3.6 Å and between intralayer vinyl groups to be 15–30 Å (Fig. 1a and Table S1†).[28] The dithiol crosslinkers were likewise modelled, and their lengths were determined to be 4.4 Å, 5.5 Å, and 6.9 Å, for 1,2-ethanedithiol, 1,3-propanedithiol, and 1,4-butanedithiol, respectively, excluding the hydrogen of the thiol (Fig. 1b and c). These calculations suggest that the dithiols are too short to form undesired intralayer crosslinks but long enough to link vinyl groups on adjacent layers (Fig. 1d).

The consumption of vinyl groups on COF-V during the thiol–ene click reactions was monitored with cross-polarization magic-angle spinning (CP-MAS) solid-state nuclear magnetic resonance (ssNMR) (Fig. 1e). Upon the addition of radical initiator (azobisisobutyronitrile; AIBN) and a dithiol to COF-V, the peaks corresponding to vinyl carbons at 133 ppm and

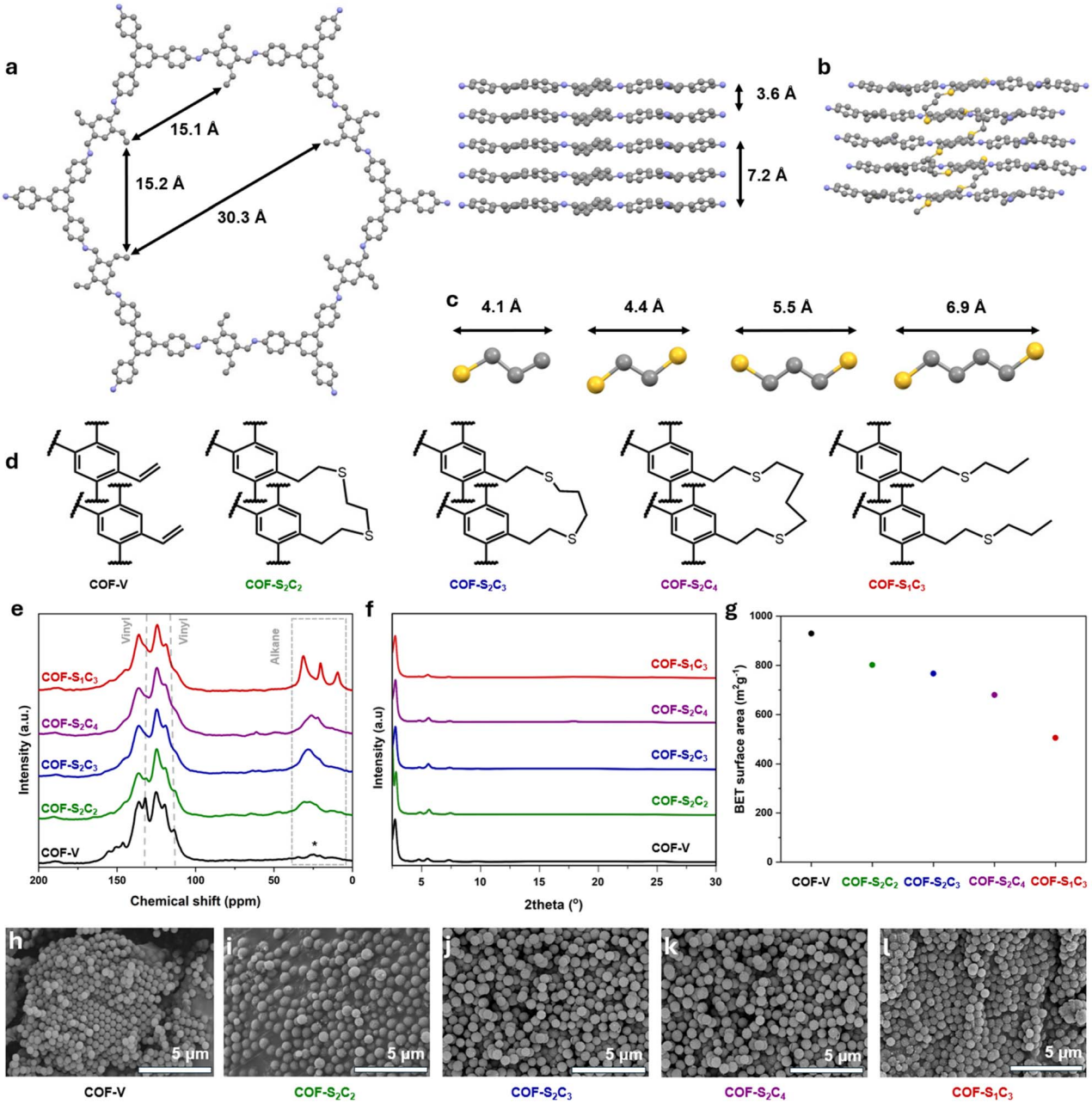

Fig. 1 (a) Simulated structure of COF-V. (b) Simulated structure of COF-S_2C_3. (c) Simulated structure of dithiol crosslinkers. (d) Chemical structures of reported materials. (e) ^{13}C CP-MAS ssNMR spectra, (f) PXRD patterns, (g) BET surface areas, and (h–l) SEM images for the reported materials.

114 ppm decrease in intensity, and a broad peak corresponding to the alkyl spacer between the thioether groups appears at 30 ppm. When COF-V is reacted with a monothiol rather than a dithiol, the resulting ssNMR spectrum shows a decrease in intensity for the vinyl peak at 133 ppm and a more clearly resolved set of peaks in the alkyl region, with peaks at 33 ppm, 22 ppm, and 11 ppm corresponding to alkyl carbons at successively further positions from the thioether group. The thiol–ene reactions were further monitored by FTIR (Fig. S9–S12†). COF-S_2C_2, COF-S_2C_3, COF-S_2C_4, and COF-S_1C_3 show a decrease in intensity for the vinyl signals at 1595 cm $^{-1}$ and 1505 cm^{-1} and the appearance of a C–H stretch at 2944 cm^{-1} from the addition of alkyl chains. In addition, no thiol (S–H) peaks were seen at 2550 cm^{-1} in the FTIR data, suggesting that both ends of the dithiol crosslinkers reacted with vinyl groups to form thioethers.[28] X-ray photoelectron spectroscopy (XPS) provided further confirmation of thioether formation (Fig. S13†). COF-S_2C_2, COF-S_2C_3, COF-S_2C_4, and COF-S_1C_3 all show the same S 2p binding energy of 163.6 eV, which has been assigned to a thioether species in the literature[34] and which indicates that the sulfur species are the same across all the frameworks. Because the monothiol-functionalized material,

COF-S_1C_3, cannot contain dangling thiol groups, the similarity of the XPS data across all the frameworks supports the absence of dangling thiol groups in the crosslinked frameworks. Elemental analysis of COF-S_2C_2, COF-S_2C_3, COF-S_2C_4, and COF-S_1C_3 revealed the sulfur content to be 3.08%, 5.72%, 4.25%, and 4.59%, respectively, suggesting that 23.0%, 44.0%, 33.7%, and 38.4% of the vinyl groups reacted, respectively (Table S2†). As discussed further below, this partial conversion of vinyl groups to thioethers successfully balances the maintenance of pore volume with the benefits of crosslinking.

To confirm the crystallinity of the COF-V derivatives, powder X-ray diffraction (PXRD) patterns were collected and compared to that of COF-V (Fig. 1f). COF-V displays a high-intensity peak at 2.74° and lower-intensity peaks at 4.76°, 5.48°, 7.30°, 9.66°, and 25.0°, which were assigned to the (100), (110), (200), (210), (220), and (001) diffractions (Fig. 1c) and are indicative of AA stacking.[28] COF-S_2C_2, COF-S_2C_3, and COF-S_2C_4 remain crystalline after the crosslinking reaction, maintaining all reflections that are present in the COF-V diffraction pattern. Notably, the interlayer spacing peak at 25.0° for COF-V shifts to a lower angle of 24.2° for the crosslinked materials, suggesting a minor expansion of the interlayer spacing upon crosslinking. On the other hand, the non-crosslinked COF-S_1C_3 shows a reduction in intensity for most of the COF-V diffraction peaks, suggesting that thioether functionalization in the absence of crosslinking may somewhat reduce crystallinity in this framework. The thermal stability of the COF-V derivatives was assessed through thermogravimetric analysis (TGA) and found to be modestly decreased compared to that of COF-V (Fig. S14–S18†), likely due to the addition of thioether-bound alkyl groups.

Gas sorption isotherms were used to probe the internal pore structure of the frameworks before and after crosslinking (Fig. 1g). Based on N_2 sorption measurements at 77 K, COF-V displays a type IV(b) isotherm[35] with a Brunauer–Emmett–Teller (BET) surface area of 930 $m^2\ g^{-1}$ (Fig. S8†). COF-S_2C_2, COF-S_2C_3, COF-S_2C_4, and COF-S_1C_3 show similar type IV(b) isotherm shapes with BET surface areas of 802 $m^2\ g^{-1}$, 767 $m^2\ g^{-1}$, 680 $m^2\ g^{-1}$, and 505 $m^2\ g^{-1}$, respectively. The pore size distribution of COF-V shows a single peak centred at 3.3 nm (Fig. S19†). COF-S_2C_2, COF-S_2C_3, COF-S_2C_4, and COF-S_1C_3 exhibit similar pore size distributions, containing a single pore centred at 3.09 nm, 3.06 nm, 3.06 nm, and 3.06 nm, respectively (Fig. S20–S23†). Complete N_2 adsorption and desorption data is given in the ESI (Fig. S24–S27†).

The significantly lower BET surface area of the non-crosslinked material COF-S_1C_3 suggests that the thioether chain extends into the pore and reduces porosity. Conversely, the higher surface areas of the crosslinked materials indicate that both thiol groups on the dithiol molecules react with vinyl groups to form interlayer cross-links, as desired, rather than bridging vinyl groups on opposite sides of a pore or leaving one end of the chain dangling into the pore. Overall, the N_2 adsorption results show that the post-synthetic crosslinking strategy provided here does not clog the pores of the parent framework.

To determine whether the post-synthetic modifications affect the nanoscale morphology of the COF-V particles, scanning electron microscopy (SEM) micrographs of COF-V and the thiol–ene derivatives were compared (Fig. 1h–l). The SEM image of COF-V shows uniform particles approximately 450–500 nm in diameter. COF-S_2C_2, COF-S_2C_3, COF-S_2C_4, and COF-S_1C_3 show similar spherical morphologies to COF-V with moderately increased particle sizes of approximately 600–700 nm. These results indicate that the dithiol crosslinkers preferentially form interlayer crosslinks rather than interparticle bridges, perhaps due to the match between the interlayer spacing (3.7 Å) and the length of the dithiol cross-linkers (4–7 Å). Thus, the thiol–ene modifications presented here do not affect the particle morphology of COF-V and instead represent a transformation of the framework lattice, converting a stack of 2D sheets into a three-dimensionally linked framework.

Chemical stability testing

Having confirmed the synthesis of the crosslinked materials, we sought to reduce the imine linkages to amines with $NaBH_4$. Linkage reduction has two major advantages: (1) increased hydrolytic stability, and (2) the installation of nucleophilic sites throughout the framework, which allows for subsequent functionalization.[6] In 3D COFs, reduction *via* $NaBH_4$ occurs without loss of crystallinity because of the robust, three-dimensionally interconnected framework.[6,16] However, in 2D COFs, $NaBH_4$ is known to cause exfoliation due to the weak non-covalent interactions that hold the sheets together, often leading to loss of crystallinity and surface area.[18–20]

Using a previously reported method of reduction for 2D COFs,[20] COF-V, COF-S_2C_2, COF-S_2C_3, COF-S_2C_4, and COF-S_1C_3 were reduced with 10.0 equivalents of $NaBH_4$ and 1.5 equivalents of glacial acetic acid at room temperature to yield a series of amine-linked frameworks termed COF-V-R, COF-S_2C_2-R, COF-S_2C_3-R, COF-S_2C_4-R, and COF-S_1C_3-R, respectively (Fig. 2a). The reduction of these materials was verified *via* FTIR and ^{13}C and ^{15}N ssNMR. By comparing the ^{13}C ssNMR spectra of COF-V and COF-V-R to the solution-state NMR spectra of small-molecule analogues, the imine carbon signal was identified at 155 ppm and was found to shift to 45 ppm after the reduction (Fig. S28†). The ^{13}C ssNMR spectra of COF-S_2C_2-R, COF-S_2C_3-R, COF-S_2C_4-R, and COF-S_1C_3-R showed the same disappearance of the imine peak at 155 ppm and appearance of the signal at 45 ppm (Fig. S29–S32†). Additional ^{15}N ssNMR data was obtained for COF-V, COF-V-R, and COF-S_2C_3-R. The COF-V spectrum shows one distinct signal at 320 ppm, corresponding to the imine nitrogen, while the COF-V-R and COF-S_2C_3-R spectra show no signal at 320 ppm and instead a single signal at 55 ppm, corresponding to the amine nitrogen (Fig. 2b). FTIR provided further confirmation of the complete reduction, showing the disappearance of the C=N stretch at 1620 cm^{-1} and the appearance of a signal at 1259 cm^{-1} and a broadened peak at 800 cm^{-1} (Fig. 2c).

The crystallinity of the reduced frameworks was examined *via* PXRD. COF-V-R shows a loss of crystallinity, retaining only the high-intensity peak at 3.02° with a sizeable amorphous halo from approximately 10–25° (Fig. 2d). Likewise, the non-crosslinked material COF-S_1C_3-R also exhibits a loss of crystallinity, evidenced by the disappearance of various low-angle

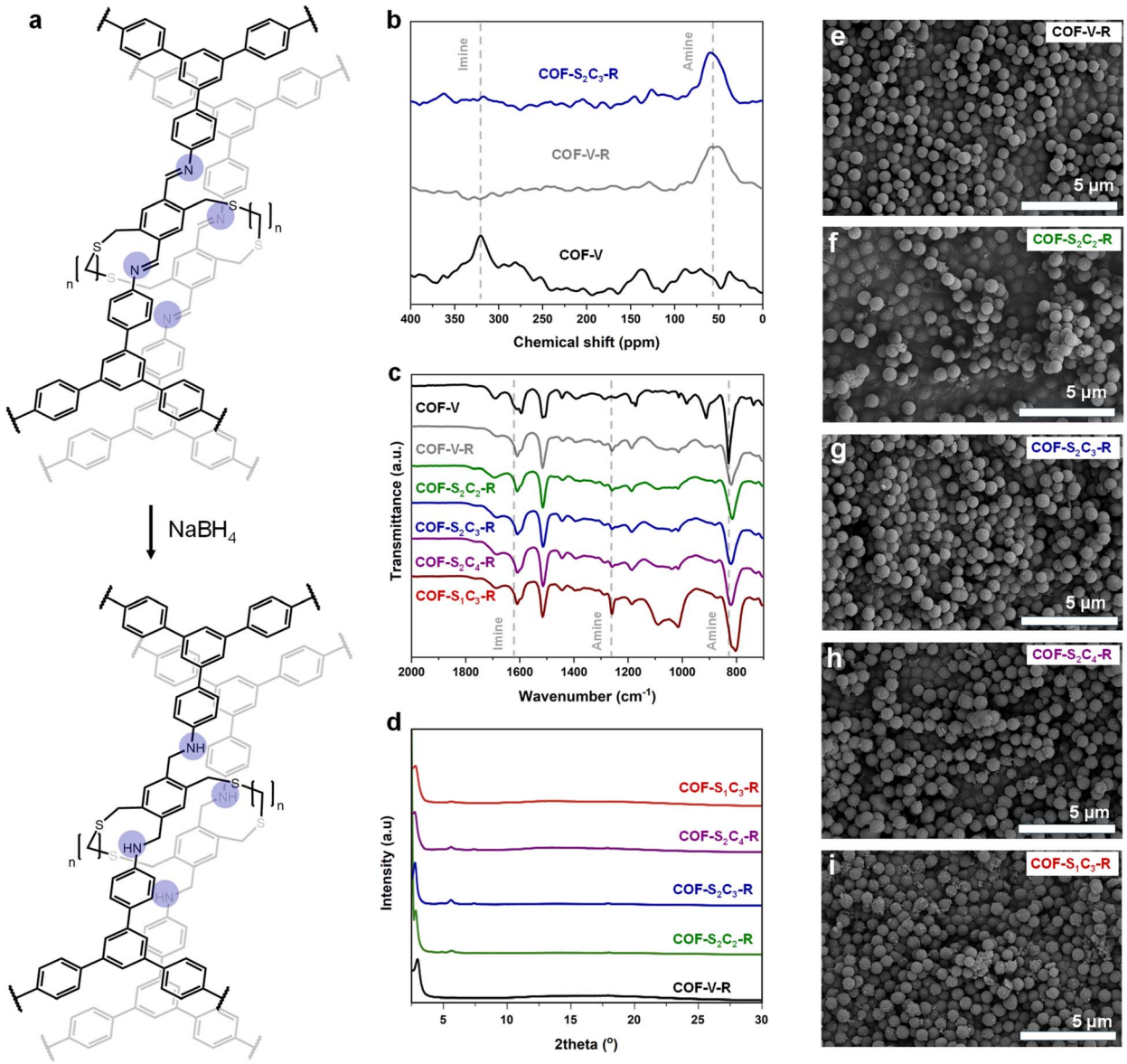

Fig. 2 (a) Chemical structure (n = 2, 3, or 4) for the crosslinked materials before and after imine reduction. (b) ^{15}N CP-MAS ssNMR spectra, (c) FTIR spectra, (d) PXRD patterns, and (e–i) SEM images for COF-V-R, COF-S_2C_2-R, COF-S_2C_3-R, COF-S_2C_4-R, and COF-S_1C_3-R.

peaks and the appearance of a sizeable amorphous halo. On the other hand, the cross-linked frameworks COF-S_2C_2-R, COF-S_2C_3-R, and COF-S_2C_4-R retain all PXRD peaks after the reduction, and both COF-S_2C_3 and COF-S_2C_4 show no amorphous halo. Thus, the increased stability from the interlayer crosslinks makes it possible to reduce the imine linkages with $NaBH_4$, a reaction previously unknown for 2D COFs. The SEM images of the frameworks after treatment with $NaBH_4$ show that the morphologies of the materials are not significantly altered (Fig. 2e–i), in spite of changes to the lattice structure seen in COF-V-R and COF-S_1C_3-R.

The benefit of thiol–ene crosslinking is most clearly seen in gas sorption measurements (Fig. 3a). When COF-V is reduced with $NaBH_4$, the BET surface area plummets from 932 $m^2\ g^{-1}$ to 10 $m^2\ g^{-1}$, the shape of the N_2 adsorption isotherm changes from type IV(b) to type II (Fig. 3a), and the pore size distribution displays multiple broadened peaks (Fig. S33†). Similarly, the BET surface area of the non-crosslinked material COF-S_1C_3 goes from 504 $m^2\ g^{-1}$ before imine reduction to only 24 $m^2\ g^{-1}$ after the reduction, the isotherm shape changes from type IVb to type II (Fig. 3a), and the pore distribution is altered and broadened (Fig. S34†). In contrast, the crosslinked materials COF-S_2C_2-R, COF-S_2C_3-R, and COF-S_2C_4-R continue to show a type IV(b) isotherm shape after imine reduction, indicating that the pore structure of the materials is preserved (Fig. 3a).[34] Further, the crosslinked materials show significantly better retention of permanent porosity after the $NaBH_4$ treatment. The BET surface areas of COF-S_2C_2-R, COF-S_2C_3-R, and COF-S_2C_4-R were calculated to be 517 $m^2\ g^{-1}$, 529 $m^2\ g^{-1}$ and 414 $m^2\ g^{-1}$, respectively, and the pore size distributions continue to show a single narrow

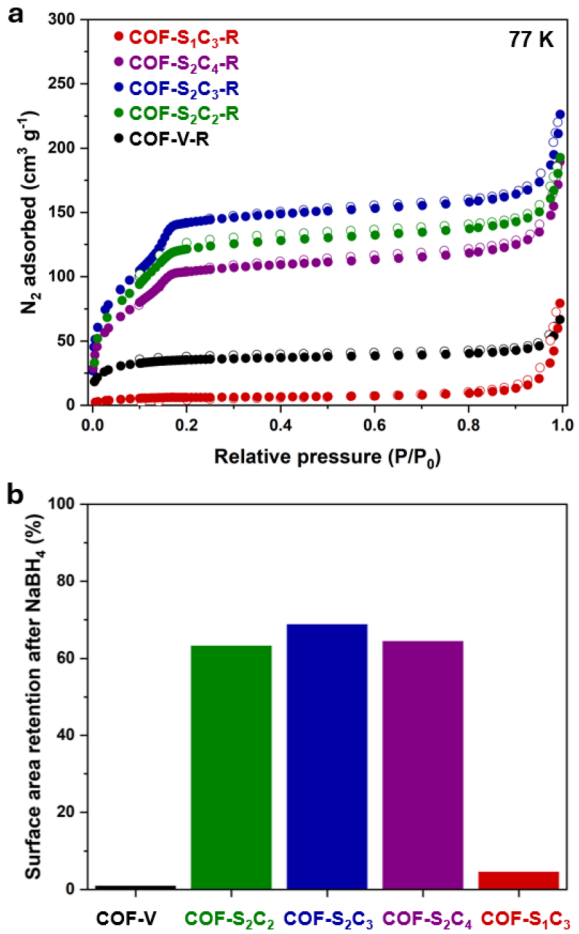

Fig. 3 (a) N_2 sorption isotherms at 77 K (filled circles show adsorption and open circles show desorption) for the reported materials after treatment with $NaBH_4$ and (b) retention of BET surface area (%) for after $NaBH_4$ treatment.

peak centred at 3.02 nm, 3.02 nm, and 3.01 nm, respectively (Fig. S35–S37†). In summary, the reduced materials exhibit BET surface areas of 1.1% (COF-V-R), 64% (COF-S_2C_2-R), 69% (COF-S_2C_3-R), 65% (COF-S_2C_4-R), and 4.7% (COF-S_1C_3-R) compared to the pre-reduction surface area for each respective material, highlighting the superior surface-area retention of the crosslinked frameworks (Fig. 3b). Considered in tandem with the PXRD outcomes discussed above, these results demonstrate that the post-synthetic crosslinking of 2D COFs increases their resistance to chemical exfoliation and degradation.

Among the crosslinked materials, COF-S_2C_3-R was selected for further study due to its superior retention of surface area and crystallinity upon $NaBH_4$ treatment. We hypothesized that crosslinking followed by linkage reduction would improve hydrolytic stability, adding to the benefits of our approach. To demonstrate the hydrolytic stability of the crosslinked, reduced frameworks, COF-S_2C_3-R and COF-V were submerged in a mixture of DMSO-d_6, D_2O, and DCl. After 24 hours, the samples were centrifuged, and the supernatant was collected and diluted with D_2O for ^1H NMR analysis. Peaks associated with the COF-V monomers (DVA and TAPB) were easily identified in the COF-V solution, showing that the inter-monomer imine linkages were hydrolyzed by the acidic D_2O solution (Fig. S38†). In contrast, no monomer peaks were found in the COF-S_2C_3-R solution, highlighting the hydrolytic stability of this framework (Fig. S38†).

Besides increasing hydrolytic stability, imine reduction liberates nucleophilic amines that can be used to further functionalize the materials. As a representative reaction, COF-S_2C_3-R was treated with 10 equivalents of acetyl chloride per amine linkage at room temperature, yielding COF-S_2C_3-Ac (Fig. 4a).[6] We showed recently that this type of nucleophilic addition can transform the adsorbate selectivity of 3D frameworks,[13] but until now, this strategy has been unfeasible for 2D frameworks due to their greater instability. ^{13}C ssNMR for COF-S_2C_3-Ac shows the appearance of peaks at 168 ppm, corresponding to the carbonyl carbon, and at 22 ppm, corresponding to the methyl carbon (Fig. 4a). As further confirmation, ^{15}N ssNMR was obtained for COF-S_2C_3-Ac, which shows the appearance of a new signal at 121 ppm corresponding to the amide nitrogen and the decrease in intensity of the amine peak

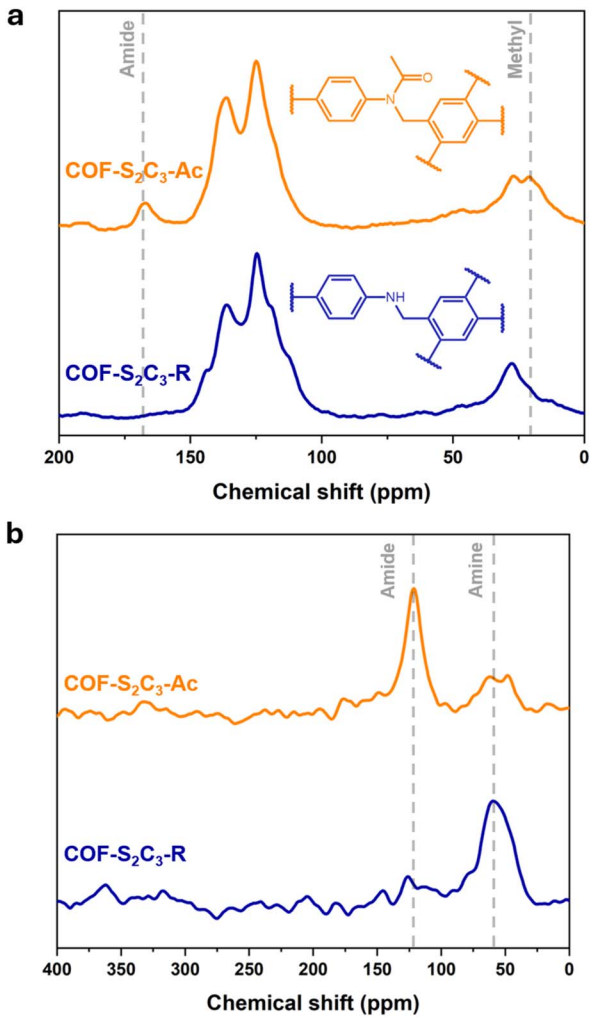

Fig. 4 (a) ^{13}C CP-MAS ssNMR spectra and (b) ^{15}N CP-MAS ssNMR spectra for COF-S_2C_3-R (blue) and COF-S_2C_3-Ac (orange).

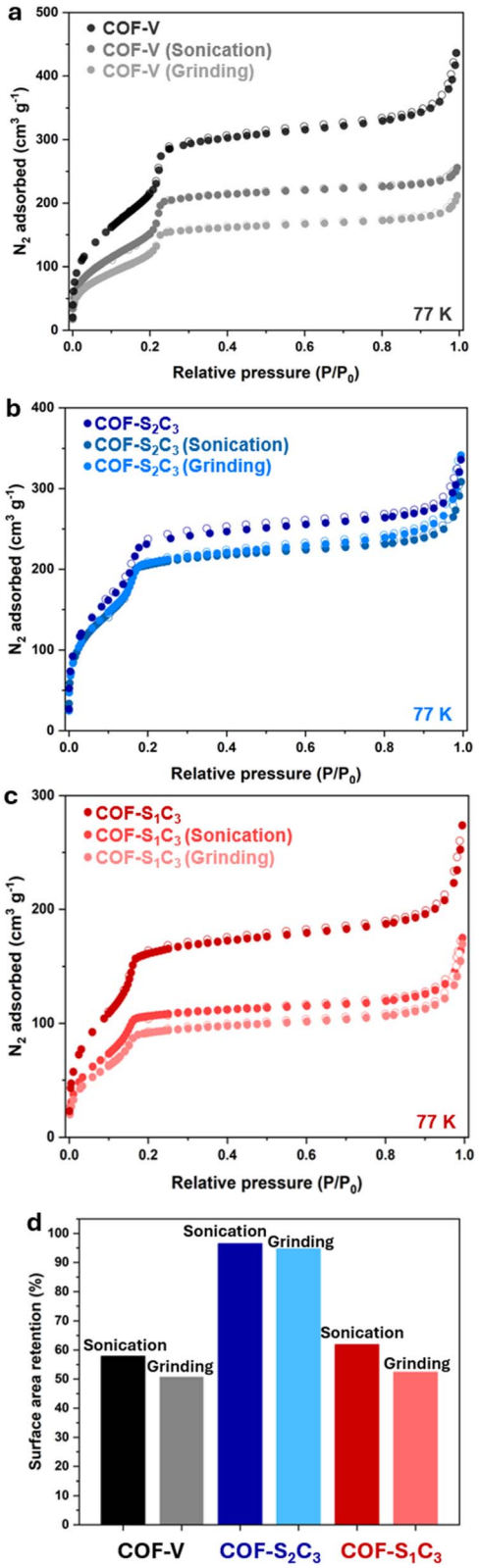

Fig. 5 N_2 sorption isotherms of (a) COF-V, (b) COF-S_2C_3, and (c) COF-S_1C_3 before and after mechanical treatment. Filled circles show adsorption and open circles show desorption. (d) Retention of BET surface area (%) after mechanical stability tests for COF-V, COF-S_1C_3, and COF-S_2C_3.

at 55 ppm (Fig. 4b). Similarly, FTIR for COF-S_2C_3-Ac shows a new signal at 1690 cm^{-1} corresponding to the amide bond (Fig. S39†). After acetylation, the crystallinity of the framework was confirmed by PXRD, showing that COF-S_2C_3-Ac maintains long-range order (Fig. S40†). The appearance of an amorphous halo from 10–28° is attributed to random orientations of crosslinks and acetyl groups and is consistent with our previous findings.[6] After acetylation, the SEM image of COF-S_2C_3-Ac shows that the framework morphology remains intact (Fig. S41†). The linkage acetylation of COF-S_2C_3 changes the gas sorption properties of the framework: COF-S_2C_3-Ac is nonporous to N_2 but shows improved CO_2 uptake compared to COF-V (Fig. S42–S45†), suggesting that functionalization of the amine linkages can be used tailor the adsorption selectivity of a crosslinked framework.

Mechanical stability tests

The mechanical stability of the crosslinked frameworks was probed in two separate tests: (1) sonicating the material in a water/ethanol solution for 30 minutes and (2) wet-grinding the material with methanol for 5 minutes. These methods have been shown to exfoliate the 2D layers of COFs, forming nanosheets and resulting in amorphous materials with reduced BET surface areas.[12–15] COF-S_2C_3 was selected as the representative cross-linked framework for these tests, and it was compared to the parent material COF-V and the non-crosslinked analogue COF-S_1C_3.

After enduring mechanical stress through grinding or sonication, COF-V, COF-S_2C_3, and COF-S_1C_3 remained highly crystalline, showing negligible change by PXRD (Fig. S46–S48†). Gas adsorption results, on the other hand, show significant divergence among the three materials as a result of mechanical stress (Fig. 5a–c). The BET surface area of COF-V was reduced to 539 $m^2\ g^{-1}$ after 30 minutes of sonication and to 473 $m^2\ g^{-1}$ after 5 minutes of grinding (Fig. 5a). Similarly, the surface area of COF-S_1C_3 was reduced to 313 $m^2\ g^{-1}$ after sonication and to 265 $m^2\ g^{-1}$ after grinding (Fig. 5c). In contrast, the crosslinked framework COF-S_2C_3 showed a negligible degree of change in surface area after the same treatment, resulting in values of 740 $m^2\ g^{-1}$ after sonication and 726 $m^2\ g^{-1}$ after grinding (Fig. 5b). To summarize these results, COF-V lost 42% of its BET surface area after sonication and 49% after grinding, COF-S_1C_3 lost 38% after sonication and 48% after grinding, and COF-S_2C_3 lost only 4% and 5%, respectively (Fig. 5d). Thus, the mechanical stability tests highlight the enhanced stability that our post-synthetic crosslinking strategy endows on a 2D COF.

Conclusions

Although 2D COFs are more widely studied and easily synthesized than their 3D counterparts, the stability of the 2D frameworks is fundamentally hampered by the lack of covalent bonds between layers. Such instability is a major obstacle preventing these otherwise promising adsorbents from enjoying the industrial prominence occupied by traditional polymers. Here, we found that a crosslinking strategy based on post-

synthetic thiol–ene reactions increases the mechanical, chemical, and hydrolytic stability of 2D frameworks. In comparison to a non-crosslinked, thiol–ene-functionalized control, the crosslinked frameworks show minimal changes to their crystalline lattice and pore structure in response to a series of chemical and mechanical stresses. Subsequent reduction of the crosslinked materials with $NaBH_4$ opens a new avenue for adsorbent functionalization by providing nucleophilic sites throughout the framework for addition to guest electrophiles. In future work, we aim to apply this approach across the broad family of 2D materials by diversifying the crosslinking chemistry and framework substrates. This approach to maximizing stability can unlock the full potential of crystalline, porous, tunable materials as industry-ready adsorbents.

Data availability

All the associated data are available in the ESI.†

Author contributions

M. K. T. and G. A. B. conceptualized the project. G. A. B. carried out all experimentation, including synthesis, characterization, and stability testing. G. A. B. and M. K. T. analyzed the data and wrote the manuscript.

Conflicts of interest

There are no conflicts to declare.

Acknowledgements

We acknowledge funding from the Gordon and Betty Moore Foundation through award #12070. We thank Dr Fu Chen and the Analytical NMR Service & Research Center at the University of Maryland for the use of NMR spectrometers (supported by award NSF-1726058). We acknowledge the support of the Maryland NanoCenter and its Advanced Imaging & Microscopy (AIM) Lab. We acknowledge the use of the Surface Analysis Center and Department of Chemistry and Biochemistry at the University of Maryland for the use of the Kratos Axis Supra instrument.

Notes and references

1 K. Geng, T. He, R. Liu, S. Dalapati, K. T. Tan, Z. Li, S. Tao, Y. Gong, Q. Jiang and D. Jiang, *Chem. Rev.*, 2020, **120**, 8814–8933.
2 S. J. Lyle, P. J. Waller and O. M. Yaghi, *Trends Chem.*, 2019, **1**, 172–184.
3 L. J. Segura, M. J. Mancheño and F. Zamora, *Chem. Soc. Rev.*, 2016, **45**, 5635–5671.
4 W. Ji, D. M. Kim, B. M. Posson, K. J. Carlson, A. C. Chew, M. Hossain, A. F. Mojica, S. M. Ottoes, D. V. Tran, M. W. Greenberg and L. S. Hamachi, *RSC Adv.*, 2023, **13**, 14484–14493.
5 A. M. Evans, M. J. Strauss, A. R. Corcos, Z. Hirani, W. Ji, S. L. Hamachi, X. Aguilar-Enriquez, A. D. Chavez, B. J. Smith and W. R. Dichtel, *Chem. Rev.*, 2022, **122**, 442–564.
6 A. N. Zeppuhar, D. S. Rollins, D. L. Huber, E. A. Bazan-Bergamino, F. Chen, H. A. Evans and M. K. Taylor, *ACS Appl. Mater. Interfaces*, 2023, **15**, 52622–52630.
7 S. O. Frimpong, N. McLane, M. Dietrich, G. A. Bauer, M. R. Baptiste, L. G. Dodson and M. K. Taylor, *Phys. Chem. Chem. Phys.*, 2024, **26**, 22252–22260.
8 X. Ma and T. F. Scott, *Commun. Chem.*, 2018, **1**, 98.
9 A. M. Evans, M. R. Ryder, W. Ji, M. J. Strauss, A. R. Corcos, A. E. Vitaku, N. C. Flanders, R. P. Bisbey and W. R. Dichtel, *Faraday Discuss.*, 2021, **225**, 226–240.
10 A. M. Evans, M. R. Ryder, N. C. Flanders, E. Vitaku, L. X. Chen and W. R. Dichtel, *Ind. Eng. Chem. Res.*, 2019, **58**, 9883–9887.
11 S. T. Emmerling, R. Schuldt, S. Bette, L. Yao, R. E. Dinnebier, J. Kästner and B. V. Lotsch, *J. Am. Chem. Soc.*, 2021, **143**, 15711–15722.
12 D. Rodríguez-San-Miguel, C. Montoro and F. Zamora, *Chem. Soc. Rev.*, 2020, **49**, 2291–2302.
13 Y. Tao, W. Ji, X. Ding and B.-H. Han, *J. Mater. Chem. A*, 2021, **9**, 7336–7365.
14 Q. Guan, G.-B. Wang, L.-L. Zhou, W. Y. Li and Y.-B. Dong, *Nanoscale Adv.*, 2020, **2**, 3656–3733.
15 F. Jin, T. Wang, H. Zheng, E. Lin, Y. Zheng, L. Hao, T. Wang, Y. Chen, P. Cheng, K. Yu and Z. Zhang, *J. Am. Chem. Soc.*, 2023, **145**, 6507–6515.
16 H. Liu, J. Chu, Z. Yin, X. Cai, L. Zhuang and H. Deng, *Chem*, 2018, **4**, 1696–1709.
17 L. Grunenberg, G. Savasci, M. W. Terban, V. Duppel, I. Moudrakovski, M. Etter, R. E. Dinnebier, C. Ochsenfeld and B. V. Lotsch, *J. Am. Chem. Soc.*, 2021, **143**, 3430–3438.
18 P. Chatterjee, A. Volkov, J. Mi, M. Niu, S. Sun, A. J. Rossini, L. M. Stanley and W. Huang, *J. Am. Chem. Soc.*, 2024, **146**, 20468–20476.
19 Q. Yan, H. Xu, X. Jing, H. Hu, S. Wang, C. Zeng and Y. Gao, *RSC Adv.*, 2020, **10**, 17396–17403.
20 S. J. Lyle, T. M. Osborn Popp, P. J. Waller, X. Pei, J. A. Reimer and O. M. Yaghi, *J. Am. Chem. Soc.*, 2019, **141**, 11253–11258.
21 X. Chen, M. Addicoat, E. Jin, L. Zhai, H. Xu, N. Huang, Z. Guo, L. Liu, S. Irle and D. Jiang, *J. Am. Chem. Soc.*, 2015, **137**, 3241–3247.
22 A. Halder, S. Karak, M. Addicoat, S. Bera, A. Chakraborty, S. H. Kunjattu, P. Pachfule, T. Heine and R. Banerjee, *Angew. Chem., Int. Ed.*, 2018, **57**, 5797–5802.
23 X. Wu, X. Han, Y. Liu, Y. Liu and Y. Cui, *J. Am. Chem. Soc.*, 2018, **140**, 16124–16133.
24 X. Li, C. Zhang, S. Cai, X. Lei, V. Altoe, F. Hong, J. J. Urban, J. Ciston, E. M. Chan and Y. Liu, *Nat. Commun.*, 2018, **9**, 2998.
25 P. J. Waller, S. J. Lyle, T. M. Osborn Popp, C. S. Diercks, J. A. Reimer and O. M. Yaghi, *J. Am. Chem. Soc.*, 2016, **138**, 15519–15522.
26 P. J. Waller, Y. S. AlFaraj, C. S. Diercks, N. N. Jarenwattananon and O. M. Yaghi, *J. Am. Chem. Soc.*, 2018, **140**, 9099–9103.

27 T. Jadhav, Y. Fang, C.-H. Liu, A. Dadvand, E. Hamzehpoor, W. Patterson, A. Jonderian, R. S. Stein and D. F. Perepichka, *J. Am. Chem. Soc.*, 2020, **142**, 8862–8870.
28 Q. Sun, B. Aguila, J. Perman, L. D. Earl, C. W. Abney, Y. Cheng, H. Wei, N. Nguyen, L. Wojtas and S. Ma, *J. Am. Chem. Soc.*, 2017, **139**, 2786–2793.
29 N. Prusinowska, M. Bardziński, A. Janiak, P. Skowronek and M. Kwit, *Chem.–Asian J.*, 2018, **13**, 2691–2699.
30 K. Yoshida, H. Takahashi and T. Imamoto, *Chem.–Eur. J.*, 2008, **14**, 8246–8261.
31 W. P. Gallagher and A. Vo, *Org. Process Res. Dev.*, 2015, **19**, 1369–1373.
32 J.-T. Ou and M. K. Taylor, *Chem. Commun.*, 2025, **6**, 11420–11426.
33 W. Sun, Y. Liu, W. Zhou, Z. Li and Z. Chen, *Talanta*, 2021, **230**, 122330.
34 X. Cao, X. Huang, J. Zeng, R. Zhang, H. Zhong and Z. Cao, *Appl. Surf. Sci.*, 2023, **608**, 155197.
35 M. Thommes, K. Kaneko, A. V. Neimark, J. P. Olivier, F. Rodriguez-Reinoso, J. Rouquerol and K. S. Sing, *Pure Appl. Chem.*, 2015, **87**, 1051–1069.